Controls on and impacts of the diurnal cycle of deep convective precipitation

C. Hohenegger[1] and B. Stevens[1]

[1] Cumulus parameterizations have well-known difficulties in capturing the diurnal cycle of tropical precipitation. This study explores the degree to which prescribed variations in cumulus mixing (entrainment/detrainment) can affect the precipitation diurnal cycle over a certain region and contribute to major climatic biases. This is achieved by artificially adjusting cumulus mixing rates as a function of time and location. It is found that variations in cumulus mixing can easily control the phase and amplitude of the oceanic precipitation diurnal cycle but not the total amount. The situation is different over land: the precipitation timing cannot be controlled by the mixing rates alone. Moreover, shifting the precipitation peak from noon to later times reduces the precipitation amplitude due to the strong diurnal cycle in convective triggering. This shift is accompanied by a reduction in net shortwave radiation and in latent heat flux (transpiration), which acts to reduce the total precipitation amount. The use of fixed SST and the absence of vegetation prevent a similar behavior over ocean. Climatic biases, as e.g., expressed by the location and structure of precipitation objects, seem not to be sensitive to the precipitation timing as long as the daily averaged precipitation remains similar. The differences are also smaller than differences induced by more structural changes performed to the convection scheme. Systematic but weak dependencies can mainly be isolated over the maritime continent, in the land-to-ocean precipitation ratio, in the location of the Atlantic ITCZ, in the surface fluxes over land, and in the net shortwave radiation.

1. Introduction

[2] With a noteworthy regularity, tropical land areas experience their first cumulus clouds in the morning hours. The clouds deepen as the day progresses and soon begin to precipitate. The convective activity culminates in the late afternoon hours before fading as the night creeps in, in the absence of organization into larger-scale disturbances [e.g., *Nesbitt and Zipser*, 2003]. Similar diurnal variations are observed over the tropical ocean, albeit of smaller amplitude and out of phase. Despite such regularity, it has long been documented that Atmospheric General Circulation Models (GCMs) have great difficulty in reproducing the correct phase and amplitude of the diurnal cycle of precipitation, both over land and ocean, as well as in the tropics and extratropics [e.g., *Dai et al.*, 1999; *Yang and Slingo*, 2001; *Collier and Bowman*, 2004; *Bechtold et al.*, 2004; *Dai and Trenberth*, 2004; *Lee et al.*, 2007b; *Dai*, 2006]. GCMs feature a systematic too early onset and peak of precipitation over land and over ocean, whereas the amplitude errors differ among the models.

[3] The characteristics of the convective diurnal cycle concisely summarize the effects of various processes involved in the convective development. Several studies have investigated the transition to deep convection by means of large-eddy simulations to disentangle such effects. Although emphasizing different processes, one common thread consists of a cloud widening as time proceeds [e.g., *Khairoutdinov and Randall*, 2006; *Kuang and Bretherton*, 2006]. Bigger clouds entrain less and thus are less inhibited from penetrating deeper in the atmosphere. These ideas are motivated by similarity arguments [*Morton et al.*, 1956; *Simpson and Wiggert*, 1969; *Simpson*, 1971] inspired and supported by laboratory experiments, wherein for idealized plumes entrainment scales wit the inverse of the plume radius. Assuming a bulk mass flux representation, as employed in typical convective parameterizations, entrainment rates can be diagnosed from large-eddy simulations.

[1]Max Planck Institute for Meteorology, Hamburg, Germany

Corresponding author: C. Hohenegger, Max Planck Institute for Meteorology, Bundesstrasse 53, DE-20146 Hamburg, Germany. (cathy.hohenegger@mpimet.mpg.de)

The derived values exhibit typical diurnal variations, in pace with the cloud depth variations [e.g., *de Rooy et al.*, 2013; *Del Genio and Wu*, 2010]. Such diurnal modulations can also be found in detrainment rates [*de Rooy et al.*, 2013].

[4] Motivated by such studies, the problem of the entrainment formulation in convective parameterizations and its possible impact on the simulated diurnal cycle of precipitation has gained renewed interest. *Wang et al.* [2007] performed regional climate model simulations over the maritime continent and increased the default (constant in space and time) value of the turbulent entrainment rate. This rectified the phase of the diurnal cycle of precipitation by 1–2 h, compared to an original 2–4 h bias, and reduced its amplitude. *Hohenegger and Bretherton* [2011] employed a combination between a buoyancy sorting algorithm and precipitation, the latter used as a predictor for the cloud area, to diagnose their entrainment and detrainment rates. Together with other modifications, they were able to improve the representation of the diurnal cycle of convective precipitation in single column model experiments. *Stratton and Stirling* [2012] modified the entrainment and detrainment formulation over land based on cloud-resolving results by *Stirling and Stratton* [2012]. Entrainment and detrainment rates were set proportional to the lifting condensation level, which serves as a proxy for the size of the thermal initiating convection, and hence cloud area. In addition, a stronger dependency between relative humidity and detrainment rate was introduced. *Stratton and Stirling* [2012] achieved a 3 h delay in the onset and peak precipitation time, which halved the phase bias. In contrast, other studies [e.g., *Lee et al.*, 2007a, 2008; *Zhang*, 2003; *Bechtold et al.*, 2004; *Xie et al.*, 2004] have focused on the triggering or closure formulation of their convection scheme and demonstrated its influence on the diurnal cycle of convection. The most notable improvement was obtained by *Rio et al.* [2009] when including the effect of cold pools on the cloud base mass flux. This eliminated the bias in the timing of the diurnal cycle of convective precipitation in single column model experiments and strongly reduced the phase bias over land in full climate simulations [see *Hourdin et al.*, 2013]. Amongst GCMs, the Institut Pierre Simon Laplace (IPSL) GCM [*Hourdin et al.*, 2013], based on the work of *Rio et al.* [2009], as well as the Met Office Hadley Centre GCM, from the work of *Stratton and Stirling* [2012] and *Stirling and Stratton* [2012], stand out with continental precipitation phase biases at least half the phase biases of other models. *Stratton and Stirling* [2012] did not modify the mixing rate formulation over ocean, whereas the IPSL results over ocean seem mixed with reduced or increased phase biases depending on location (from a visual inspection of Figure 17 in *Hourdin et al.* [2013]).

[5] Building on such results, this study aims to systematically explore the interplay between cumulus mixing, the characteristics of the convective diurnal cycle, and the resulting simulated climate. The two specific questions addressed by this study are: (i) To what extent can spatio-temporal variations in entrainment/detrainment affect the diurnal cycle of precipitation? And (ii) To what extent do changes that influence the diurnal cycle of precipitation also influence other aspects of the simulated climate? Both issues are important to guide and prioritize parameterization development. The present work focuses on the deep tropics, between 15°S and 15°N. In evaluating the results, attention is given to the overall precipitation climatology, expressed not only by precipitation amounts but by the location and extent of its main precipitation objects.

[6] The applied methodology differs from the above-mentioned studies. *Wang et al.* [2007] and some of the sensitivity studies on closure/triggering have applied time-invariant and spatially uniform perturbations to specific control parameters of the convection scheme, that were also constant in space and time. *Stratton and Stirling* [2012] or *Rio et al.* [2009] and some others have introduced state-dependent relationships which can be motivated physically. Here, an approach in-between these two extremes are followed. Turbulent entrainment and detrainment rates, which were usually spatially and temporally uniform, are perturbed according to a pre-defined spatio-temporal pattern. The latter depends upon the grid location and elapsed integration time, but not on the simulated flow. For instance, by reducing cumulus mixing at a given time or place, convection can be favored relative to other locations and times where mixing rates are specified to be larger.

[7] Such an approach is clearly not physically based, nor was it ever contemplated to implement such an approach permanently into the model. The mixing rates are artificially varied in space and time, in a manner loosely based on variations seen in large-eddy simulations, to serve three other purposes. First, it avoids the problem of biases in the prediction of the required flow-dependent variables contaminating the results. This often explains why improvements in full global climate model simulations are more difficult to achieve than in the better constrained single column model experiments. Second, it allows an easier identification and assessment of spatio-temporal effects, e.g., the importance of the continental diurnal cycle of precipitation for the oceanic mean precipitation climate. This is especially true as both convection and specific parameterization choices are known to impact and interact in quite complicated ways with their environment [e.g., *Bony and Emanuel*, 2005; *Bacmeister et al.*, 2006; *Möbis and Stevens*, 2012] through the ambiguous dependence between precipitation and vertical velocity, precipitation and cloud radiative effects, or between precipitation and surface flux feedbacks. Third, and foremost is the thought that before developing complex models to justify spatio-temporal variations in mixing rates, it is worth exploring the potential impact of such changes in a simpler, easier to control, set up. Sensitivities revealed in this fashion can then help focus development efforts.

[8] The outline of the paper is as follows. Section 2 describes in more detail the GCM used and especially its convection scheme, as well as the design of the experiments, and the observational data sets. The results are presented in sections 3–5. Section 3 deals

with the question of control on the diurnal cycle of deep convective precipitation and section 4 assesses the climatic impacts of the precipitation diurnal cycle. Whereas sections 3 and 4 concentrate on the effects of temporal variations in mixing rates with spatially compact support, section 5 allows the temporal variations to spatially differ. The results are discussed in section 6 and conclusions are presented in section 7.

2. Method

2.1. ECHAM

[9] The simulations are performed with the latest version of the atmospheric GCM ECHAM, ECHAM6 coupled to the land surface model JSBACH. Details on the model and on its ability to reproduce the Earth climate are given in *Stevens et al.* [2013]. The default convection scheme in ECHAM6 is the TNT (Tiedtke-Nordeng-Tiedtke) scheme described by *Möbis and Stevens* [2012] and based on work by *Tiedtke* [1989] and *Nordeng* [1994]. Because the scheme plays a central role in this study some of its important elements are reviewed in more detail below.

[10] The TNT scheme employs a classical bulk entraining-detraining plume. Updraft mass flux M_u and updraft properties ψ_u are parameterized as

$$\frac{dM_u}{dz} = M_u(\varepsilon - \delta) \tag{1}$$

$$\frac{d\psi_u}{dz} = \varepsilon(\overline{\psi} - \psi_u) + S \tag{2}$$

with ε entrainment rate (m^{-1}), δ detrainment rate (m^{-1}), $\overline{\psi}$ mean environmental property, and S source term.

[11] The scheme distinguishes between three types of convection: shallow, midlevel, and deep. They differ in their triggering, closure, as well as entrainment and detrainment formulation. Shallow convection is the dominant type of convection happening over tropical ocean in ECHAM simulations following the AMIP protocol. It typically occurs 67% of the time the scheme is active. (Here and in the following the terms tropics/tropical refer to the latitudinal band 15°S to 15°N.) Deep convection constitutes 20% of the convective events, and the remaining 13% of the events are classified as midlevel convection. The corresponding frequencies over the tropical landmasses are 35%, 15%, and 50%. The convection scheme itself contributes to 95% of the total tropical precipitation, distributed in 77% deep, 13% shallow, and 10% midlevel events.

[12] Triggering shallow or deep convection requires moisture convergence in the subcloud layer to be positive, the updraft humidity at cloud base to be more than 1% higher than the humidity of the environment and for the diagnosed updraft to be positively buoyant. The first updraft computation employs a nonentraining plume including a perturbation of the updraft temperature at cloud base. The perturbation is proportional to the standard deviation of the temperature at the lowest model level. If the moisture convergence exceeds the surface evaporation by more than 10% and the resulting clouds are more than 200 hPa deep, deep convection is triggered. Otherwise shallow convection occurs. If neither shallow nor deep convection is triggered, midlevel convection may be activated in levels higher than 1500 m above the surface providing the following two conditions are met: the environmental relative humidity exceeds 90% and large-scale upward motion is present.

[13] In terms of the closure, shallow convection employs a moisture convergence closure. The mass flux at cloud base is set proportional to the moisture convergence within the subcloud layer. Deep convection makes use of a closure that relaxes the convective instability to zero over a specified timescale. For midlevel convection, the cloud base mass flux is determined by the strength of the vertical mass transport by the large-scale flow.

[14] Entrainment and detrainment include the contribution of two processes, a turbulent and an organized exchange. The first one parameterizes the small-scale turbulent mixing of cloudy and environmental air at the cloud edges. The second one characterizes larger scale and organized entrainment/detrainment of air in and out of the cloud associated with, for instance, the acceleration of the upward mass flux through the cloud. Turbulent entrainment $\varepsilon_{\text{turb}}$ and detrainment δ_{turb} rates are equal in magnitude. Their values are set to 0.1 km^{-1} for deep and midlevel convection and 0.3 km^{-1} for shallow convection. Above half the cloud depth or higher if the cloud is too thin or if the level of the maximum environmental vertical velocity lies higher than half the cloud depth, $\varepsilon_{\text{turb}}$ is switched off so that the mass flux decreases with height. Organized entrainment ε_{org} and detrainment δ_{org} rates only exist for deep convection. ε_{org} is proportional to the vertically integrated buoyancy of the updraft. δ_{org} is distributed between the lowest possible organized detrainment level and the cloud top height so as to reduce the mass flux following a predefined profile. The lowest possible organized detrainment level mainly depends upon the updraft buoyancy.

[15] In order to get a better sense of the different entrainment/detrainment terms, Figure 1 shows as an example vertical profiles of δ_{turb}, ε_{org}, and δ_{org} averaged over 1 month. Only tropical oceanic points with an updraft top above 8 km are considered to avoid that organized detrainment from shallower clouds contaminates the lower portion of the profile. Remember that $\varepsilon_{\text{turb}} = \delta_{\text{turb}}$ over the lower half of the cloud layer and that $\varepsilon_{\text{turb}}$ vanishes in the upper half. ε_{org} dominates around cloud base before rapidly decreasing and almost vanishing in the upper half part (>5 km) of the cloud layer. In contrast, δ_{org} increases with height and attains its maximum value around 10 km. Averaged below and above 6 km, ε_{org} and δ_{org} amount to 0.1 km^{-1}. They are thus of comparable magnitude to $\varepsilon_{\text{turb}}$ and δ_{turb}.

[16] The TNT convective parameterization in the standard ECHAM set up does not employ a complex representation of cloud microphysical processes. A certain fraction of cloud water/cloud ice is converted at each level to precipitation. Precipitation can evaporate below cloud base. Finally, in complement to its updraft model, the scheme includes a downdraft model. The
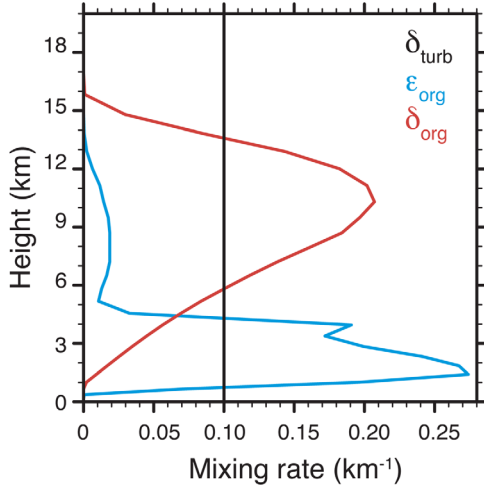
Figure 1. Vertical profiles of entrainment and detrainment rates in the standard ECHAM model as averaged over 1 month and over tropical (15°S to 15°N) oceanic points with a cloud top above 8 km.

downdraft starts at the level of free sinking with a mass flux proportional to the cloud base mass flux.

2.2. Experimental Set Up

[17] A large number of simulations with systematic spatio-temporal variations in cumulus mixing rates are performed. Only the values of ε_{turb} and δ_{turb} for deep convection are perturbed, whereby the standard TNT procedure is followed: δ_{turb} is set equal to ε_{turb} and ε_{turb} is switched off above half the cloud depth or higher (see section 2.1). Hence, changes to the TNT scheme can be completely typified by describing how ε_{turb} is changed in a particular simulation, a convenience that will be adopted in the remaining of this manuscript. All the simulations are integrated with the ECHAM6 LR configuration, characterized by a spectral truncation of T63 and 47 vertical levels, and with fixed sea surface temperature (SST). The latter design follows the AMIP protocol. Simulations are integrated for 5 years (1978–1982), except when noted otherwise.

[18] The first experiment, named CTL, refers to the simulation performed with the standard ECHAM model configuration, as described in section 2.1. No spatio-temporal modifications are imposed, i.e., $\varepsilon_{turb} = 0.1$ km^{-1}. CTL is identical to the integration

Table 1. Overview of the Simulations[a]

Name	T_o	ε_l	Name	T_l	ε_o	Name	T_o	T_l
P18o	0	0.1	P18l	0	0.1	P02oP14l	8	20
P22o	4	0.1	P22l	4	0.1	P14oP02l	20	8
P02o	8	0.1	P02l	8	0.1	P02oP02l	8	8
P06o	12	0.1	P06l	12	0.1	P14oP14l	20	20
P10o	16	0.1	P10l	16	0.1	P22oP14l	4	20
P14o	20	0.1	P14l	20	0.1	P06oP14l	12	20
						P18oP14l	0	20
						P10oP14l	16	20

Name	ε_o	ε_l	Name	ε_o	ε_l
CTL	0.1	0.1	TUNo	$1.1+0.4\cdot\sin((t-20)\frac{\pi}{12})$	0.1

[a]If $T_{o,l}$ is indicated, $\varepsilon_{o,l}$ is computed using equation 3. Otherwise, it is constant and takes the listed value. Units for $\varepsilon_{o,l}$ are here km^{-1} and for $T_{o,l}$ h. Suffix o stands for ocean, l for land. The simulations P??o and P??l have been repeated with organized entrainment and organized detrainment turned off. The latter are called P??o_nog and P??l_nog.

called ECHAM6-LR which formed the basis of the analysis in *Stevens et al.* [2013].

[19] The design of the remaining simulations is such that it allows exploring to what extent ε_{turb}, by controlling its diurnal phase as well as spatial pattern, can control the phase of the diurnal cycle of deep convective precipitation over distinct regions and the overall climatology. As discussed in section 1, the purpose of such changes is not to suggest changes to parameters for possible operational use, but rather to uncover specific sensitivities of the convection scheme and of the simulated precipitation field.

[20] Three groups of experiments are performed (see Table 1). The first two serve to investigate the impact of an ε_{turb} temporally varying over a certain region. The last group explores the effects of temporal variations in ε_{turb} that differ in space. The basic naming convention is P??o (first group), P??l (second group), and P??oP??l (third group). The characters o and l indicate the region over which ε_{turb} is perturbed: ocean only in P??o, land only in P??l, both ocean and land in P??oP??l. The acronym P?? characterizes the imposed temporal variations. ε_{turb} is specified to undergo a sinusoidal modulation of period 24 h, with a phase P of ?? h. The two question marks (or wild cards) typify the time ε_{turb} attains its minimum value. The concrete formulation of ε_{turb} thus reads:

$$\varepsilon_{turb}(x,y,t)=\begin{cases}\varepsilon_o=2\cdot10^{-4}\left(1.1+\sin\left((t-T_o)\frac{\pi}{12}\right)\right) & \text{for oceanic points}\\[2mm]\varepsilon_l=2\cdot10^{-4}\left(1.1+\sin\left((t-T_l)\frac{\pi}{12}\right)\right) & \text{for land points}\end{cases} \tag{3}$$

[21] $T_{o,l}$ (h) are constants, whereas t denotes hours from local midnight. The resulting entrainment values are in m^{-1}.

[22] The values chosen for $T_{o,l}$ are listed in Table 1 and the ensuing time varying $\varepsilon_{o,l}$ are illustrated in Figures 2a and 2b. The use of a sinusoidal curve is an

obvious choice given the overall form of the diurnal cycle of precipitation (see e.g., Figure 4) and results from large-eddy simulations on the transition phase to deep convection (see section 1). During the decay phase, mixing rates are also found to increase in large-eddy
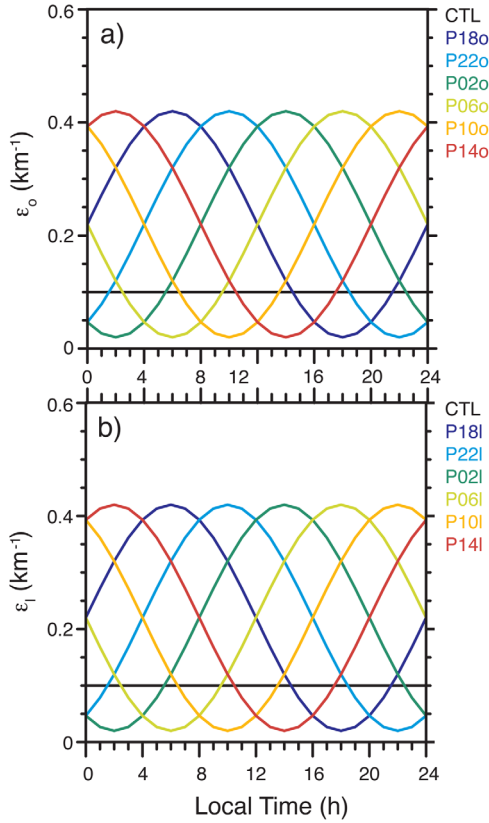
Figure 2. Diurnal cycles imposed on (a) ε_o and (b) ε_l. Only ε_o is modified in the Figure 2a experiments, ε_l is set to 0.1 km^{-1}. Similar is true for the land experiments in Figure 2b. Remember that $\varepsilon_{turb} = \delta_{turb}$ and ε_{turb} vanishes roughly above half the cloud depth.

simulations, although the variations tend to be smaller. Tests have also been performed with a step function and gave similar results. As implied by equation 3 and as evident in Figures 2a and 2b, a relatively large amplitude is prescribed. The motivation for doing so is to maximize the impacts of $T_{o,l}$ on the diurnal cycle of deep convection. The dependency of the results on this particular choice is discussed when appropriate in the remainder of the text.

[23] As noted earlier, equation 3 only alters the formulation of deep convection. However, implementing similar modifications to the midlevel or shallow convection does not affect the conclusions of this study. This is not surprising given that most of the convective precipitation is of deep origin.

[24] One weakness of the chosen experimental set up is that the results may be dependent on the detailed formulation of the TNT scheme. In particular because the TNT scheme has both organized (ε_{org} and δ_{org}) and turbulent (ε_{turb} and δ_{turb}) mixing, changes in one may be compensated for by changes in the other. To address this limitation and in an effort to have a more general view of the results, the P??o and P??l experiments are repeated with the organized entrainment and organized detrainment set to zero. The two new sets of simulations are referred to as P??o_nog and P??l_nog. Furthermore,

turning off ε_{org} and δ_{org} constitutes a more profound modification to the TNT scheme than imposing a diurnal cycle in ε_{turb}. This provides another useful measure to asses the significance of the changes induced by variations in $T_{o,l}$.

[25] A last and special simulation, called TUNo, is performed. TUNo employs a ε_l of 0.1 km^{-1} and a ε_o given by $1.1 + 0.4 \cdot \sin\left((t-20)\frac{\pi}{12}\right)$ km^{-1}. These peculiar choices result from the analysis of the P??o and P??l simulations and are thus justified in section 3.

2.3. Model Evaluation

[26] The experiments of Table 1 are contrasted to evaluate the extent to which changes in the timing of precipitation are associated with other changes in the statistics of the resultant climate. The changes are objectively assessed using Taylor diagrams [*Taylor*, 2001] and a variant of SAL [*Wernli et al.*, 2008]. These scores are not presented for their operational guidance, as generally done, but for their quantitative insight as to the model sensitivities. With respect to the precipitation field, significant differences are those that are on the order of the inherent model biases, or at least on the order of the differences between paired simulations in P??o and P??o_nog or P??l and P??l_nog using the same ε_{turb}. This implies that, although ε_{turb} may alter the precipitation field over a certain region, the impact may not be significant and, given this definition, ε_{turb} not seen as a way to ameliorate major biases in the model climatology.

[27] The simulated precipitation climatology is mainly evaluated in terms of its multiyear mean and interannual variability. Consideration of shorter timescales enhances the differences among the simulations. Spatially, the precipitation field is compared globally and over specific regions (or subdomains). They are identified in Figure 3 which also presents the mean precipitation climatology from the Global Precipitation Climatology Project (GPCP) version 2 [*Adler et al.*, 2003]. The ten defined subdomains consist of: Atlantic (ATL), Africa (AFR), Indian Ocean (INO), Asia (ASI), Maritime continent (MAR), south Pacific (SPA), west Pacific (WPA), east Pacific (EPA), Central America (CAM), and south America (SAM). The subdomains, especially the maximum precipitation that they were designed to enclose, emerge almost naturally by isolating regions of strong precipitation in the GPCP data. Local maxima occur in GPCP (by decreasing order of magnitude) over New Guinea (MAR), the Columbian coast (CAM), Indonesia (MAR), northwest Pacific (WPA), the Brazilian coast (SAM), northeast Pacific (EPA), Indian Ocean (INO), south Pacific (SPA), Amazon (SAM), Atlantic (ATL), Gulf of Guinea (AFR), and Vietnam (ASI). Regrouping the Brazilian coast and Amazon maxima as well as the New Guinea and Indonesia maxima yields the ten subdomains of Figure 3. The chosen subdomains also partly overlap with the ones used by *Nesbitt and Zipser* [2003]. Four of them (ATL, EPA, WPA, and SPA) are purely oceanic, two (AFR and SAM) are purely continental, and four
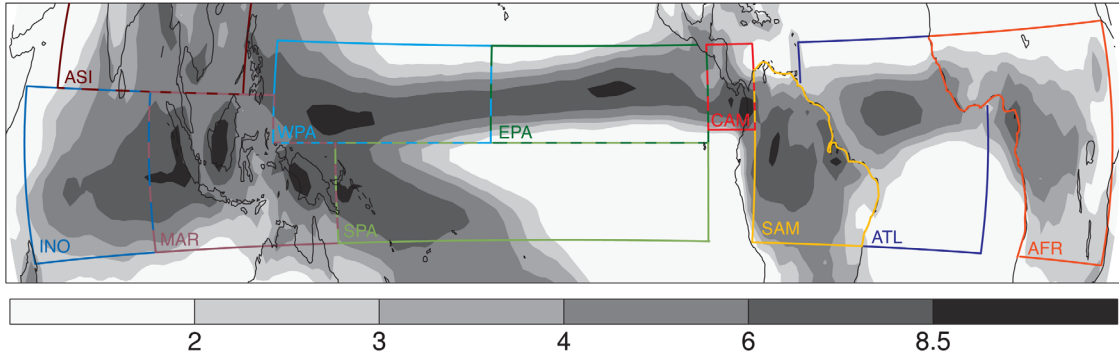
Figure 3. Overview of the chosen subdomains overlaid on the GPCP mean precipitation climatology (mm day^{-1}). The subdomains are Atlantic (ATL: 60°W–0°E, 15°S–15°N), Africa (AFR: 20°W–40°E, 15°S–15°N), Indian Ocean (INO: 50°E–90°E, 15°S–7°N), Asia (ASI: 60°E–120°E, 7°N–35°N), Maritime continent (MAR: 90°E–150°E, 15°S–7°N without the square 130°E–150°E, 0°N–7°N), south Pacific (SPA: 150°E–90°W, 15°S–0°N), west Pacific (WPA: 130°E–160°W, 0°N–15°N), east Pacific (EPA: 160°W–90°W, 0°N–15°N), Central America (CAM: 90°W–75°W, 2°N–15°N), and south America (SAM: 75°W–30°W, 15°S–15°N). SAM and AFR are restricted to land points only, WPA, EPA, SPA, and ATL to oceanic points only.

(INO, ASI, MAR, and CAM) cover both land and ocean.

[28] Since GPCP only provides daily resolution, precipitation observed from the Tropical Rainfall Measuring Mission (TRMM, see *Huffman et al.* [2007]) is considered when assessing the diurnal cycle of precipitation. TRMM supplies precipitation on a 3 hourly resolution. Both GPCP and TRMM were interpolated to T63L47 resolution for purposes of comparison, whereas TRMM was linearly interpolated in time to 1 h resolution.

3. Controls on the Diurnal Cycle

[29] Figure 4 shows the monthly mean diurnal cycle of precipitation averaged over tropical ocean for the experiments with modifications in ε_o only, and over tropical land for the experiments with ε_l perturbations. The P??o_nog and P??l_nog experiments are not displayed in Figure 4 and not discussed in this section as they exhibit an identical behavior. Perturbing ε_{turb} only over the ocean does not significantly affect the mean diurnal cycle of precipitation over land and vice versa for P??l. Note also that here and in the following, the term amplitude is employed to characterize the difference between the daily maximum and minimum of a given quantity. The term daily averaged precipitation refers to the precipitation averaged over the duration of a simulation.

[30] Focusing first on the six P??o simulations and comparing Figures 4a and 2a, it is evident that the diurnal cycle of precipitation tends to follow the timing imposed through ε_o, as was anticipated by the experimental design. Precipitation maximizes at the time ε_o reaches its minimum and a 4 h phase shift in ε_o induces a corresponding 4 h phase shift in precipitation. The amplitude of the diurnal cycle of precipitation varies only weakly among the six simulations, although there is a tendency for the simulations with daytime precipitation peak (P14o and P18o) to exhibit a weaker ampli-

tude. Similar results are obtained when shifting T_o at another given amplitude in ε_o, as long as the imposed amplitude is not too small. The limiting case happens around a value of 0.02 km^{-1}, corresponding to a
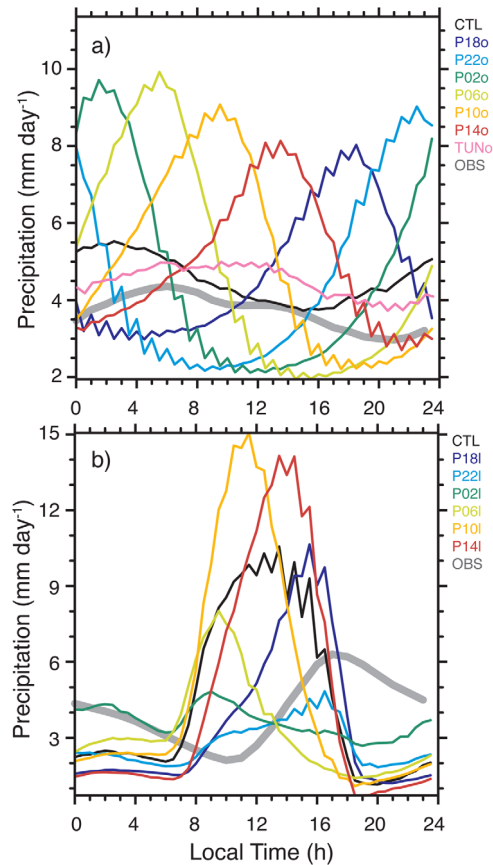

Figure 4. Monthly mean diurnal cycle of precipitation (mm day^{-1}) for various experiments averaged over tropical (a) ocean and (b) land. Thick gray line for TRMM observations.
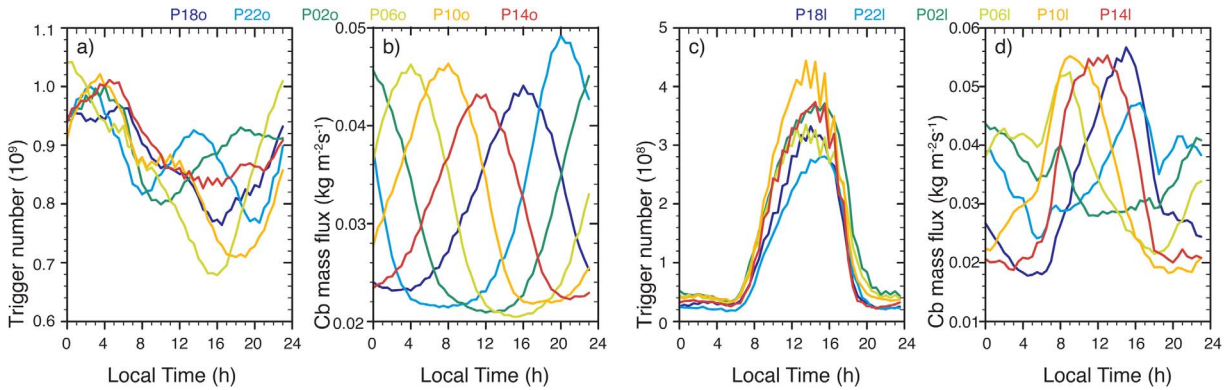
Figure 5. Monthly mean diurnal cycle in (a and c) deep convection occurrence and (b and d) mean cloud base mass flux (kg m^{-2} s^{-1}) averaged over tropical (Figures 5a and 5b) ocean for P??o and (Figures 5c and 5d) land for P??l.

precipitation amplitude of ~1.1 mm day^{-1}. Below this, values of ε_o are too small to be able to limit the development of convection and the curves collapse toward CTL.

[31] Comparison of Figures 4a and 2a also indicates that, although the P??o simulations have a mean entrainment rate ε_o twice as large as CTL, they produce very similar (5.1 mm day^{-1}) daily averaged precipitation. Factors other than ε_{turb} have to play a more dominant role in constraining the mean precipitation amounts over ocean, as explained further below.

[32] Over land the response of convective precipitation to changes in ε_{turb} differs from the response over the ocean (see Figure 4b). Shifting the time of minimum ε_l by 4 h still retards the time of maximum precipitation, but by various lags depending on T_l. None of the simulation is able to produce a nighttime precipitation peak, resulting in an aliasing of the peak precipitation time onto the daytime hours (~8–20 LT) irrespective of the entrainment formulation. The amplitude and daily average of the diurnal cycle of precipitation strongly respond to a change in T_l. In particular, forcing a late afternoon/nighttime precipitation peak, as with P22l or P02l, yields a strong reduction in precipitation amplitude and daily averaged values.

[33] Figure 4 also displays in gray the mean diurnal cycle of precipitation derived from TRMM. From the above discussion, it is relatively easy to tune ε_o to match the TRMM curve over ocean. However, given that the observed precipitation amplitude only slightly exceeds the 1.1 mm day^{-1} threshold, this proves more challenging in practice. TRMM nevertheless likely underestimates the amplitude of the diurnal cycle of precipitation due to its 3 hourly resolution.

[34] An example of such a tuned simulation, denoted by the abbreviation TUNo, is shown in magenta in Figure 4a. Both the resulting precipitation phase and amplitude appear quite realistic despite a slightly too pronounced secondary maximum near 12 LT. Although the ε_o values specified in TUNo can correct for phase and amplitude biases, the precipitation amounts remain too large. It is not clear as to how much concern to

attach to this discrepancy as the accuracy of precipitation retrievals over ocean remains a matter of some debate [e.g., *Stephens et al.*, 2012]. The observed and simulated time periods also do not match. In any case and as indicated previously, tuning of ε_o cannot reduce the simulated daily averaged oceanic precipitation.

[35] The mean diurnal cycle of precipitation over land cannot be reproduced from entrainment rate variations alone. Various phases, amplitudes, and functions for ε_l have been tried. They all fail for the same reason, i.e., both a correct timing and amplitude of the precipitation signal cannot be simultaneously achieved as delaying the onset of precipitation through an artificial change in entrainment rate negatively impacts the amplitude of precipitation. *Lee et al.* [2007b] also observed a strong reduction in amplitude when delaying the onset of convection by making it harder for the convection scheme to convect through modifications in the trigger formulation.

[36] The tendency over land of phase changes to be aliased onto the daytime hours of the diurnal cycle of precipitation, in contrast to the ocean, can be understood by examining the triggering frequency of deep convection and the evolution of its cloud base mass flux (see Figure 5). Together with ε_{turb}, they essentially determine the precipitation evolution. Deep oceanic convection can easily be triggered at any time of the day in ECHAM (see Figure 5a). The temporal variations are small and so are the variations across the simulations. Note that using diurnally varying SSTs would actually flatten the diurnal cycle of convection triggering even more since the warmer SSTs during the late afternoon could correspondingly enhance the convective activity. Likewise (Figure 5b), the cloud base mass flux does not seem to be limited by the time of the day and may peak at any time. Combination of these two effects explains the relative insensitivity of the precipitation amplitude to phase changes.

[37] Moreover studies have shown that parameterized convection tends to be quite sensitive to the latent heat flux [e.g., *Hohenegger et al.*, 2009]. Ultimately and in a global sense, precipitation acts to balance the latent

heat flux. As will be shown and explained in section 4.2, the latent heat flux does not vary much over ocean with a daily averaged value around 142 W m^{-2} (or 4.9 mm day^{-1}), close to the simulated daily averaged precipitation of 5.1 mm day^{-1}. This imposes a strong constraint on ECHAM with the consequence that the chosen ε_o only acts to redistribute the 5.1 mm day^{-1} throughout the day.

[38] Convection over land undergoes in contrast a strong diurnal cycle. All the simulations exhibit a clear and very similar preference to trigger convection between 8 and 20 LT in Figure 5c. The integrations with minimum ε_l during night, i.e., P22l, P02l, and P06l in Figures 5c and 5d, exhibit larger mean cloud base mass flux and slightly more frequent triggering than P10l, P14l, and P18l, but the values remain below the maxima attained between 8 and 20 LT. This explains the shortage in nighttime precipitation despite strongly reduced ε_l and the resulting flatter precipitation amplitude. More specifically, comparing the values of cloud base mass flux, triggering frequency and precipitation at the time of minimum ε_l suggests that the strong reduction in nighttime triggering primarily explains the corresponding reduction in precipitation. Convection is for instance triggered 18× less frequently in P22l compared to P14l (at 22 LT and 14 LT, respectively), precipitation is 7× smaller, but the reduction in cloud base mass flux only amounts to a factor of 1.4.

[39] As an additional effect and in opposition to the ocean, the latent heat flux ends up varying between the simulations, with differences of up to 25 W m^{-2} or 0.86 mm day^{-1} (see section 4.2). A phase shift from midday to later times reduces the latent heat flux. This feeds back on the convection scheme, on the simulated precipitation amounts, and explains the strong reduction in daily averaged precipitation in e.g. P22l or P02l. The hydrological cycle can sustain different daily averaged precipitation amounts, whereby precipitation decreases by 1.3 mm day^{-1} per 1 mm day^{-1} decrease in latent heat flux. This yields daily averaged precipitation amounts of 3.1, 2.65, 2.7, 3.2, 3.9, and 3.9 mm day^{-1} in P18l, P22l, P02l, P06l, P10l, and P14l. These differences are important to bear in mind to understand the climatic impacts of the diurnal cycle as discussed in the next section.

[40] Figure 5b also highlights that, over ocean, the evolution of the cloud base mass flux recalls the precipitation evolution in Figure 4a and thus its relationship to the prescribed ε_o. The time of maximum cloud base mass flux is shifted by 4 h from one to the other simulation and occurs 2 h before the time of maximum precipitation and minimum ε_o. The same holds over land in Figure 5d as long as the convection can easily be triggered, i.e., during daytime. A large ε_{turb} prevents convection to develop and to release the instability. Since TNT employs a CAPE closure, the cloud base mass flux correspondingly increases. When ε_{turb} finally allows convection, CAPE is consumed and the cloud base mass flux decreases as well. It is nevertheless surprising that cloud base mass flux and ε_{turb} are so strongly coupled.

[41] In terms of parameterization development (and based on these results) it appears that, at least the difficulty of the TNT scheme to capture the diurnal cycle of precipitation observed over land, can to a large extent not be ascribed to entrainment. Larger entrainment rates in the morning and a reduction toward midday are needed to delay the precipitation onset and peak, but modifications in the triggering and/or closure are necessary to generate enough late-afternoon and nighttime precipitation. As will be shown in the next section, biases in the daily averaged precipitation rate are a more acute problem than a wrong phase of the diurnal cycle. These findings may reflect a weakness in the representation of the midlevel convection in TNT, which, in theory, should supplement deep convection during night. Although it cannot be excluded that the findings presented in this section may result from a peculiar behavior of ECHAM, the aliasing onto daytime hours would in theory tend to speak for an approach as adopted by *Rio et al.* [2009] who obtained a correct diurnal cycle of precipitation in single column model experiments by coupling the closure of their convection scheme to a gust front parameterization. More generally, the analysis presented in this section supports a combination of both diurnally varying mixing rates and enhanced late afternoon/nocturnal precipitation through adequate closure/triggering modifications, as ventured in *Hohenegger and Bretherton* [2011]. Over ocean, phase and amplitude biases can be eliminated through an appropriate specification of the entrainment rate, although it cannot be excluded that similar effects may be achieved by controlling other aspects of the convection scheme (e.g., closure). The daily averaged precipitation nevertheless tends to remain unaffected, at least for the type of entrainment perturbations tested here.

4. Climatic Impacts of the Diurnal Cycle

[42] Some of the possible climatic impacts of the diurnal cycle of deep convection are assessed in this section by comparing the climatology resulting from the different experiments with each other and to observations. Over ocean, TUNo captures the correct amplitude and timing of the diurnal cycle of precipitation, but, as any other P??o simulations, overestimates the daily averaged precipitation. Over land, none of the simulations listed in Table 1 is able to simultaneously reproduce the precipitation phase, amplitude, and daily average. P22l exhibits a nearly correct phase, P06l and P18l simulate a more realistic amplitude, whereas P10l and P14l tend to capture the daily averaged precipitation. Contrasting the climatic responses between these three subgroups can thus help understand the degree to which major climatic biases may be associated with one or the other aspect of the simulated diurnal cycle. Moreover, consideration of the simulations characterized by an obviously wrong diurnal cycle of precipitation (e.g., P02l or P14o) is of importance as one would expect such simulations to exhibit the largest discrepancies relative to observations. Finally, it is interesting to assess to what extent
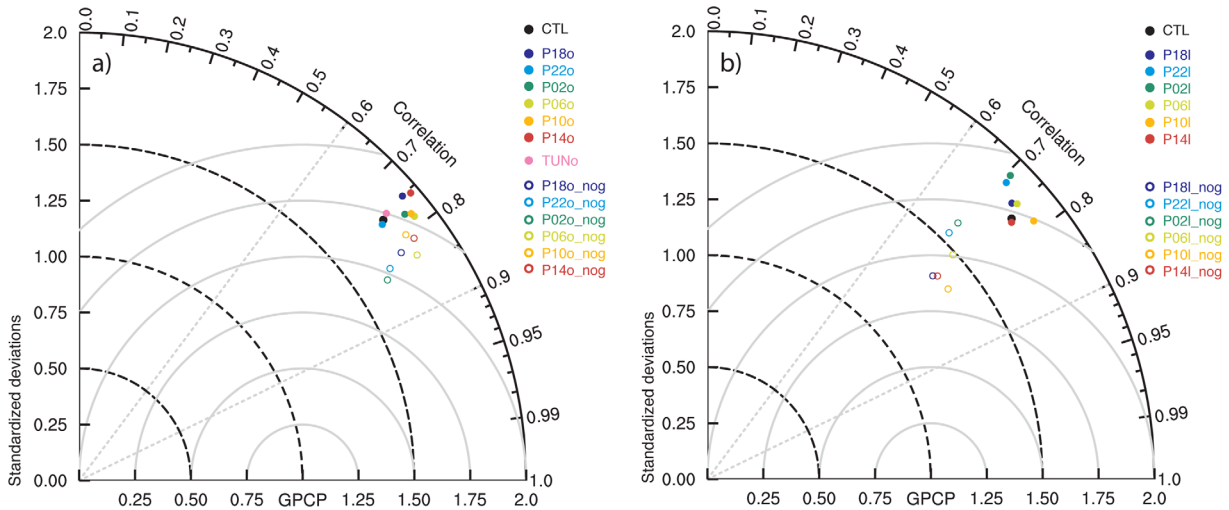
Figure 6. Taylor diagrams based on 5 years (1978–1982) of precipitation simulated over the tropics for simulations with (a) ε_o and (b) ε_l perturbations. The reference data set stems from GPCP.

systematic changes in the climatology can be identified in the experiments, thereby suggesting a particular dependency of convection in one or the other region on the nature of its diurnal cycle either there or elsewhere.

4.1. Precipitation

[43] Figure 6 shows two Taylor diagrams to assess the mean error characteristics of the annually averaged tropical precipitation in the various experiments (see *Taylor* [2001] for a description of Taylor diagrams). Only the tropical region comprised between 15°S and 15°N and the precipitation averaged over the years 1978–1982 (except by GPCP with respect to the time period) are considered. This restricted spatial and temporal averaging explains the poorer agreement of CTL with GPCP as compared with Figure 8 in *Stevens et al.* [2013], for which the correlation is 0.85. Extension to longer timescales tends to reduce the distance to GPCP but not the spread among the points, at least for the few experiments that were integrated up to 20 years.

[44] Over ocean (Figure 6a), shifting the time of maximum precipitation seems to have a comparatively modest effect. The P??o simulations are much more similar to each other and to TUNo than to GPCP or to the simulation in the P??o_nog group using same ε_{turb}. The P??o_nog simulations exhibit a similar behavior, albeit with a slightly larger spread among them. The changes in the error measures from one to the other simulation tend to be in the range of 10–15% for P??o and 15% for P??o_nog, whereas the inherent model biases are more than 100% depending on the error measure. P14o, characterized by a clear daytime precipitation peak, barely stands out as less skillful.

[45] Over land, the spread inside the P??l and P??l_nog groups is enhanced. The integrations tend to cluster as a function of the daily averaged precipitation, i.e., abundant (P10l and P14l) versus weak (P02l and P22l). This suggests that the differences in skill visible in Figure 6b

follow from the variations in precipitation amounts rather than from the shift in peak precipitation time per se. Or, shifting the phase by conserving the daily averaged precipitation (e.g., P10l versus P14l) has relatively little effect, in agreement with the behavior over ocean. This also suggests that, given the current TNT formulation, capturing a correct phase or amplitude of the diurnal cycle of precipitation by sole control of ε_{turb} has a detrimental impact on the precipitation climatology, at least given the skill measures considered here.

[46] Figure 7 presents the precipitation signal for specific regions, as outlined in Figure 3 and section 2.3. The design of Figure 7 is inspired from the skill score developed by *Wernli et al.* [2008], which aims at validating the amplitude, structure, and location components of the precipitation field separately. Figure 7 focuses on the structure and location components, as expressed by the extent and mean center of mass of precipitation objects. The latter are defined as connected regions with precipitation amounts bigger than 70% of the maximum precipitation in each subdomain. Using local maxima instead of the global maximum over the global tropics is deemed necessary for the ECHAM simulations due to the excessive amounts of precipitation falling over the Pacific region. Also, a simulation-dependent threshold avoids contamination of the structure/location signal by amplitude errors [*Wernli et al.*, 2008]. The amplitude component does not provide any supplementary insights and is not discussed.

[47] The high similarity that exists between the integrations, both in terms of the location and extent of the precipitation objects, constitutes the most remarkable feature of Figure 7. It is striking how all the simulations produce a precipitation object that lies along the coast of northeast Brazil instead of the central Atlantic. The simulations miss the coastal maximum over the Gulf of Guinea yielding a southeastward shift of the center of mass into the African inland. Similar is true over South
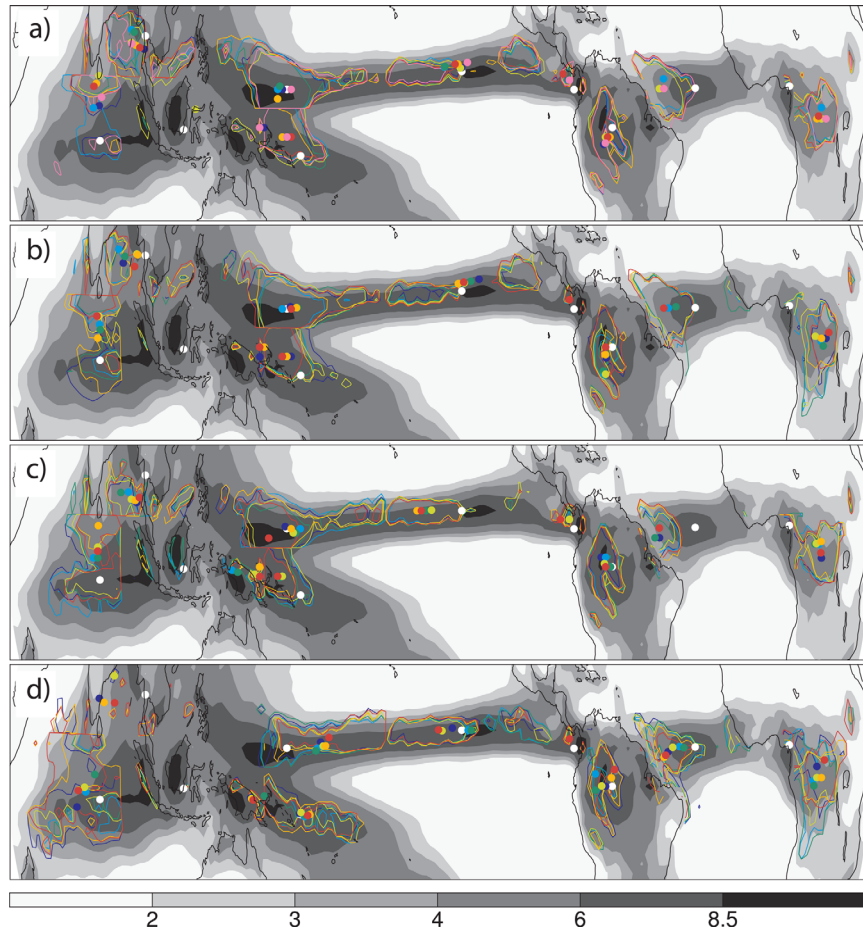
Figure 7. GPCP mean precipitation (shading, mm day^{-1}), precipitation extent (contour lines), and location of weighted center of mass (symbols) in (a) P??o and TUNo, (b) P??l, (c) P??o_nog, and (d) P??l_nog. Colors as in previous figures, the white full circles stand for GPCP. For each of the subdomains defined in Figure 3, precipitation objects are isolated according to $RR > 0.7\ RRmax$, with RR precipitation and $RRmax$ maximum precipitation in a subdomain. The corresponding outline of each such object is made visible by the contour lines, whereas the location of the mean center of mass of all objects in one subdomain is rendered by the symbols. To compute the mean center of mass, the center of mass of each object is weighted by the amount of precipitation per object.

America. The spread between the simulated precipitation objects is larger around the maritime continent (see INO and ASI) but does not encompass GPCP. ECHAM performs especially poorly over MAR with centers of mass lying near the Papua-New Guinea coast and no precipitation object detected over Borneo. This follows from anomalously high precipitation falling along the Papua-New Guinea coast. The apparent improvement in the location of the mean center of mass over MAR in P06o purely results from the production of a second rain maximum along the coast of Sumatra. Finally, the Pacific ITCZ, especially in SPA, WPA, and CAM, tends to exhibit a northward shift and further biases in the number, location and extent of precipitation objects in all the simulations as compared to GPCP.

[48] Although a control of the time of peak precipitation through a control of the TNT mixing rates does not seem to project onto the overall tropical precipitation biases, some consistent and systematic (albeit moderate) dependencies upon the nature of the diurnal cycle of precipitation do emerge. First, the extended region around the maritime continent in P??o, P??o_nog, P??l, P??l_nog is most sensitive to the timing of the diurnal cycle of precipitation (see Figure 7). Second, the P??l_nog and, to a lesser extent, the P??l experiments exhibit a systematic shift of the ATL center of mass away from the Brazilian coast in proportion to a reduction of the daily precipitation amounts over the continents. Such an improvement of the ATL center of mass would unfortunately mean a degradation of the simulated precipitation over SAM, suggesting that a sole modulation of ε_{turb}, and/or the use of too simple perturbations may not be sufficient to improve the overall precipitation distribution.

[49] Figure 8 illustrates a third and last consistent response of the mean precipitation field in terms of a systematic variation of the land-to-ocean precipitation
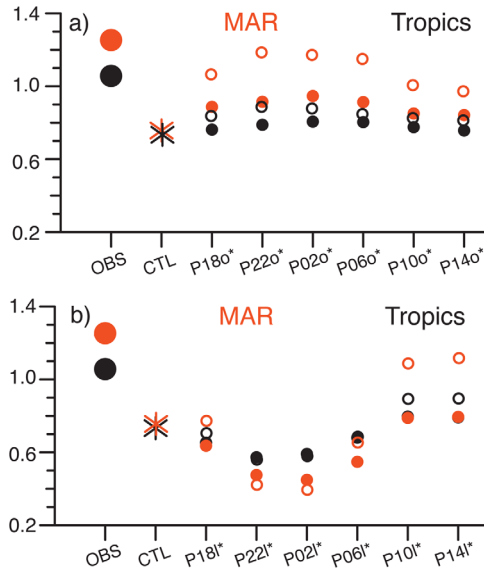
Figure 8. Ratio between continental and oceanic precipitation falling in the tropics and in subdomain MAR for GPCP observations, CTL as well as (a) P??o (full circles) and P??o_nog (circles) and (b) P??l (full circles) and P??l_nog (circles).

ratio with imposed phase. Shifting the time of peak oceanic precipitation from day (12 LT) to night (0 LT) enhances the land-to-ocean precipitation ratio (Figure 8a). The opposite is true over land.

[50] The different sensitivity of the land-to-ocean precipitation ratio to phase shifts over land versus ocean reflects the distinct nature of the diurnal cycle over the latter two regions, as alluded in section 3. The land-to-ocean precipitation ratio increases if the rain amounts falling over land increase. This requires a daytime precipitation peak for the case of ε_l perturbations. In P??o and P??o_nog, on the other hand, a depletion of the precipitation amounts falling during daytime over ocean is needed to avoid that precipitation is favored over the ocean relative to the land. This preferred state happens with a nighttime precipitation peak. The sensitivity is relatively weak considering the whole tropics but is more pronounced over specific subdomains like MAR.

[51] Moving away from the mean climatology toward its variability with a computation of interannual precipitation variability from a set of simulations that were integrated out to 20 years yields results akin to the behavior of the mean precipitation: a modest change amongst the simulations as compared to the typical simulations biases, similar dependency upon the imposed phase in P??o,l and P??o,l_nog as well as larger discrepancies when organized entrainment/detrainment are turned off. For a specific month, precipitation statistics were also outputted every 30 min to explore possible modifications in intensity-frequency relationships. Specifying the phase of the oceanic diurnal cycle of precipitation does not alter the intensity-frequency relationship (not shown). Over land, shifting the precipitation peak from noon to later times reduces the

frequency of events experiencing more than 30 mm day^{-1} of precipitation. The reduction in convective frequency is partly compensated by the occurrence of more frequent, but stronger, nonconvective rain events. The different sensitivity to changes over ocean versus land is not inconsistent in the sense that shifting T_l can suppress convection during limited periods of time, in contrast to T_o which only shifts the precipitation amounts in time (see section 3).

4.2. Other Climatic Impacts

[52] Figure 9 shows the components of the surface energy budget averaged over tropical ocean for P??o and tropical land for P??l, and expressed as differences to CTL. The *_nog groups exhibit similar changes in the components of the surface energy budget, albeit with slightly larger differences, and are not displayed for clarity. Changes over the ocean for P??l and over land for P??o are small, in agreement with the spatially confined modifications in ε_{turb} and the ensuing confined precipitation perturbations (section 4.1).

[53] The shortwave cloud radiative effect (CRE) varies by as much as $\sim$10 W m^{-2} across the simulations, whereas changes in the longwave CRE are more modest (see Figure 9). Interestingly the simulations which tend to rain most during day (e.g., P14l versus P02l or P10o versus P22o) experience an increase in net shortwave radiation. Despite stronger precipitation or rather because of the stronger precipitation, the integrated cloud liquid water content is more strongly depleted in those integrations. Comparing all simulations, changes in CRE are primarily in pace with changes in integrated cloud liquid water content rather than with changes in cloud cover. This produces systematic variations in net shortwave radiation as function of the imposed $T_{o,l}$, as clearly visible in Figure 9.

[54] The differences in CRE impact sensible and latent heat fluxes over the land areas (Figure 9b). Noteworthy is that variations in sensible and latent heat fluxes turn out to be anticorrelated. The latent heat flux for instance increases by 24 W m^{-2} going from P02l to P14l, whereas the sensible heat flux decreases by 12 W m^{-2}. The implied change in Bowen ratio points to the behavior of the vegetation as simulated by JSBACH. The ε_l specification allows P14l to rain more than P02l,
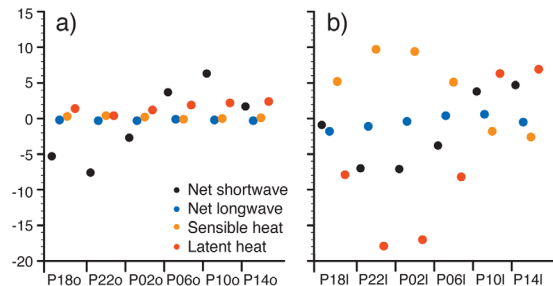

Figure 9. Differences in net shortwave flux at the surface, net longwave flux at the surface, sensible heat, and latent heat relative to CTL averaged over tropical (a) ocean for P??o and (b) land for P??l. Units in W m^{-2}.
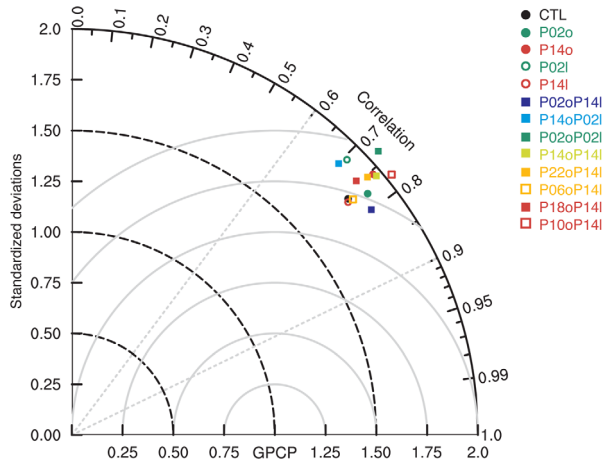
Figure 10. Same as Figure 6 but for the experiments with diurnal cycles of various phases combined over land and ocean.

hence increasing soil moisture and, as explained above, the amount of radiation available for photosynthesis. Both of these changes provide more favorable conditions for plants and their transpiration is enhanced. The Bowen ratio shifts in favor of the latent heat flux. Given that the increase in latent heat flux over consumes the energy surplus, the sensible heat flux decreases and the surface cools by $1°C$. Cooler 2 m air temperatures can favor plant growth depending on its optimum temperature, which may further enhance the latent heat flux.

[55] Over ocean, the use of fixed SST as well as the absence of vegetation prevent a strong response of the surface heat fluxes despite the variations in CRE between the simulations.

5. Spatio-Temporal Variations in the Diurnal Cycle of Deep Convection

[56] Sections 3 and 4 focused on the effects of a temporally varying ε_{turb}, with temporal variations restricted to either the ocean or the land. Here, the possible climatic impacts of spatially varying phases of the convective diurnal cycle are investigated. This is achieved by combining distinct T_o and T_l, see the simulations denoted by P??oP??l in Table 1. The latter combinations serve as a surrogate for the use of state-dependent entrainment rates and can help illustrate the optimal characteristics of the land versus oceanic diurnal cycle of precipitation that such state-dependent relationships ought to capture, or at least the capacity of such changes to influence the simulations as a whole.

[57] Figure 10 summarizes the results in form of a Taylor diagram, similar to Figure 6. P02oP14l and P14oP02l constitute the two extreme combinations. P02oP14l forces a nighttime peak over ocean and a daytime peak over land. This represents the combination of the best individual simulations with respect to precipitation amount and land-to-ocean precipitation ratio (see section 4). Not surprisingly, P02oP14l stands out as the most skillful experiment in Figure 10. It is also slightly

more skillful than P02o or P14l taken separately. P14oP02l, with its forced daytime peak over ocean and nighttime peak over land, personifies the worst scenario. It is also the least skillful integration in Figure 10 in terms of correlation coefficient, even though the loss in correlation only amounts to 0.1. Comparison of P02oP02l to P14oP14l further indicates that the degradation in skill in P14oP02l primarily follows from forcing a nighttime peak over land and from the associated reduction in daily averaged precipitation.

[58] Inspection of the remaining simulations reveals further, albeit minor, differences. At least from a land-to-ocean precipitation ratio perspective, there is a clear tendency of increased ratio with increasing lag between the time of peak precipitation over land and over ocean. An increased lag especially avoids that the ocean, where convection can be easily triggered, steals rain from the land. For some of the experiments, this translates itself into a point lying nearer GPCP in Figure 10. But as in section 4, the spatial distribution of precipitation remains mostly unchanged.

[59] The P??oP??l experiments can also be employed to isolate the best phase combination for each of the ten subdomains. Such a combination is identified by the simulation with the smallest precipitation difference to GPCP. The results do not reveal any consistent picture. A best phase combination over a subdomain often performs poorly over another one.

6. Discussion

[60] The findings in the previous sections tend to emphasize that major precipitation biases in ECHAM do not strongly relate to the specific characteristics of the simulated precipitation timing as long as the daily averaged precipitation remains approximately conserved. The minor nature of the precipitation response is especially striking in P??o. Over ocean and as compared to perturbations applied to ε_l, the overall precipitation amounts are relatively insensitive to the way entrainment is parameterized, likely as a consequence of the flat diurnal cycle in convective triggering and cloud base mass flux. Also, the use of fixed SST and the absence of vegetation avoid a strong response of the latent heat flux to a change in the surface energy budget (through CRE), preventing a strong feedback of the latent heat flux on the developing convection. Although in all the simulations changes in precipitation are very well correlated with changes in the 500 hPa vertical velocity and thus the large scale, the changes are relatively small. Turning off organized entrainment/detrainment removes one possibility for the convection scheme to compensate for the imposed changes, thus allowing for larger differences.

[61] It is still surprising that a shift in timing cannot impact more significantly the large-scale circulation, especially through the a priori expected changes in shortwave heating rate. The latter are presumably too small and spatially too uniform (given the use of spatially uniform perturbations in ε_l or ε_o) to alter the large-scale circulation.

[62] The findings are also not inconsistent with the results of previous studies that were able to improve certain characteristics of the simulated climate by improving the physical representation of their entrainment rates [e.g., *Chikira*, 2010] or to partly associate specific model biases, like the double ITCZ, to the entrainment formulation [e.g., *Möbis and Stevens*, 2012; *Oueslati and Bellon*, 2013]. As can be deduced from the land experiments, a first step toward impacting the precipitation climatology requires a significant change in the daily averaged precipitation. Based on this study and for the reasons given above, it nevertheless seems unlikely that playing with the phase of the diurnal cycle of precipitation and its control through ε_{turb} can achieve this. Moreover, *Chikira* [2010] or *Möbis and Stevens* [2012] more drastically altered their entrainment formulation. Comparing the simulations with same ε_{turb} but on/off organized entrainment confirms that a more fundamental change to the entrainment formulation can have a significant impact on a global measure of the precipitation skill, even over ocean. Such structural changes are nevertheless not needed to control the timing of precipitation given sufficient triggering of convection and cloud base mass flux.

[63] The question remains whether the weak sensitivity may be limited to an evaluation of the TNT model, with little basis for generalizing to other models of convection. The design of the experiments was chosen so as to remain as faithful as possible to routine climate simulations performed with ECHAM, e.g. in the framework of CMIP. Also, despite the use of simple perturbations, significant changes could be observed in the characteristics of the diurnal cycle of precipitation in Figure 4 and section 3, which seem just not able to project onto the mean climate in section 4. Furthermore, the *_nog simulations, which employ a structurally different version of TNT, exhibit similar dependencies upon the imposed phase of the precipitation diurnal cycle. Clarification on parameterization effects could be best attained by repeating such type of analysis with other climate models. For the Met Office Hadley Centre GCM, the results of *Stratton and Stirling* [2012] seem to confirm that a delayed (by 3 h) continental diurnal cycle of precipitation is not able to modify the spatial distribution of precipitation. *Lynn et al.* [2004] examined regional climate model change experiments over the United States for a couple of summer seasons using two different cumulus parameterizations, one promoting daytime and one nighttime precipitation. They found a distinct warming over the United States that they ascribed to the distinct precipitation phase. On one hand, this is not so different from the response observed between P14l and P02l. On the other hand, the use of two different cumulus parameterizations entails much more fundamental changes to the representation of convection than solely perturbing the entrainment rate. Their precipitation field not only differs by the simulated precipitation phase but also its intensity and spatial distribution.

[64] The overall weak sensitivity may also be an expression of an absence or misrepresentation of the processes through which the diurnal cycle could impact the precipitation climatology. Many studies have for instance documented the diurnal propagation of the convective signal from the land to the adjacent ocean [*Yang and Slingo*, 2001] or from the mountains to the plains [*Carbone and Tuttle*, 2008]. Such propagation generally does not occur in coarse-resolution climate models. It also assumes a correct link between clouds and convection, which cannot be guaranteed and indeed seems unlikely.

[65] Finally, it merits noting that the obtained precipitation sensitivity, already weak, is likely overestimated. Due to the changes in shortwave CRE, the integrations exhibit radiative imbalances at the top of the atmosphere. Climate models get tuned to remove such imbalances [*Hourdin et al.*, 2013; *Mauritsen et al.*, 2012]. *Mauritsen et al.* [2012] in particular showed that, using different sets of tuning parameters, one of them being the chosen ε_{turb} value for shallow convection, similar mean climates can be produced. Because it is unclear if such tuning would amplify or damp the signal of the response, some of the experiments were tuned to ensure a zero radiative imbalance at the top of the atmosphere and integrated again. The response of the diurnal cycle of precipitation to perturbations in $T_{o,l}$ remains similar, but the climatic impacts, especially the variations in precipitation amounts or the temperature changes, are reduced.

7. Conclusions

[66] This study explored the interplay between parameterization choices, convection characteristics, and simulated climate. The focus was set on the problem of the diurnal cycle of precipitation over the tropics and the role of entrainment/detrainment in this respect. More specifically, the extent to which a biased diurnal phase in the diurnal cycle of deep convective precipitation is due to a misrepresentation of cumulus mixing rates was investigated by allowing the latter to vary in space and time in a controlled way. In a second step, the importance of the specific characteristics of the diurnal cycle of precipitation, in terms of its phase, amplitude, and spatial variations thereof, for the simulated mean climate was assessed. All the simulations were performed with the ECHAM6 GCM using prescribed SSTs.

[67] Results indicate that over ocean the phase and amplitude of the diurnal cycle of precipitation can easily be modulated by introducing appropriate temporal variations in the cumulus mixing rates, as long as the simulated precipitation amplitude is larger than 1.1 mm day^{-1}. The daily averaged precipitation amounts remain mostly unaffected for the set and kind of perturbations tested. This is not true over land. Imposing a late precipitation peak, in better agreement with observations, drastically reduces and negatively affects both the daily averaged precipitation and the precipitation amplitude because the convection scheme is in the first place not able to sustain convection. In particular, deep convection is not triggered at night and midlevel convection appears ineffective.

[68] In terms of climatic impacts and major model biases, the simulated phase and spatial variations thereof of the diurnal cycle of precipitation appear of secondary importance. Despite widely differing characteristics in their diurnal precipitation patterns, all the performed integrations reproduce a similar distribution of precipitation with nearly identical location and structure of their main precipitation objects. The differences induced by a phase shift of the diurnal cycle of precipitation appear also smaller than the differences induced by a structural change (turning off organized entrainment and organized detrainment) introduced in the TNT convection scheme. A global measure of precipitation skill shows clear deterioration only in those cases where the phase shift is accompanied by a strong decrease of the daily averaged precipitation, as observed over land in some of the simulations. The deterioration may thus be viewed as related to the simulated precipitation amounts rather than their timing per se.

[69] Although the climatological distribution of precipitation does not strongly respond to phase shits, some systematic but moderate responses nevertheless emerge. The land-to-ocean precipitation ratio, the daily averaged precipitation amounts falling over land, the location of the Atlantic ITCZ as well as the components of the surface energy budget exhibit such more systematic responses. The net shortwave radiation at the surface increases with a phase shift from night to day due to a reduction of the integrated cloud liquid water content. Over land, the sensible heat flux decreases with a phase shift from night to day, whereas the latent heat flux increases. This follows from the changes in the available net shortwave radiation at the surface and the response of the vegetation (transpiration) to such changes.

[70] The overall weak sensitivity, the weaker sensitivity over ocean than over land, the changes in precipitation amplitude and daily averaged precipitation over ocean versus land can all be understood from the nature of the diurnal cycle of deep convection over land and over ocean as well as from the response of the latent heat flux. Over land, the strong diurnal cycle in convection triggering mostly prevents convection to develop during night, strongly reducing the precipitation amplitude in those simulations with high daytime ε_l values. The ensuing reductions in net shortwave radiation at the surface and in latent heat flux feed back on the convection scheme and sustain a positive feedback with a reduction of the daily averaged precipitation amounts. In opposition, oceanic regions exhibit a flat diurnal cycle in convection triggering (and cloud base mass flux) and relatively constant latent heat flux due to the use of fixed SST and the absence of vegetation.

[71] From a parameterization point of view, the findings suggest that a correct representation of the diurnal cycle of precipitation over land both requires temporally varying mixing rates and, more importantly, appropriate modifications in the convective closure/trigger formulation to allow the production of enough nocturnal precipitation. Temporally varying mixing rates are sufficient to control the phase and amplitude

of the oceanic diurnal cycle of precipitation, even though their values do not affect the daily averaged precipitation. Benefits can be expected over land areas in those simulations that are able to favor continental precipitation. Capturing the right daily averaged precipitation appears in this context much more crucial than reproducing the observed phase. An enhancement of land precipitation requires in the current set up diurnal cycles that are 12 h out of phase between land and ocean with a precipitation peak around 14 LT over land, or, otherwise, would require changes in the closure and/or trigger formulation.

[72] Due to the obtained overly weak sensitivity, the findings suggest that introducing spatio-temporal variations in cumulus mixing rates to control and improve the diurnal cycle of precipitation, can only weakly project onto the simulated mean climate. Also, the possibly achieved improvements seem often to deteriorate other aspects of the climate, calling for more structural changes in the representation of convection. All in all, there may thus not be any magic bullet for widely improving precipitation in GCMs, but rather several aspects of the parameterization likely need to be addressed, including feedbacks between the convection dynamics and parameterization choices. Given the relatively weak effect of varying the precipitation phase on the mean climate through varying the mixing rates, it might be worth to systematically explore the effects of such other aspects.

References

Adler, R. F., et al. (2003), The version-2 Global Precipitation Climatology Project (GCPC) monthly precipitation analysis (1979-present), *J. Hydrometeorol.*, *4*, 1147–1167.

Bacmeister, J. T., M. J. Suarez, and F. R. Robertson (2006), Rain reevaporation, boundary layer-convection interactions, and pacific rainfall patterns in an AGCM, *J. Atmos. Sci.*, *63*, 3383–3403.

Bechtold, P., J.-P. Chaboureau, A. Beljaars, A. K. Betts, M. Köhler, M. Miller, and J.-L. Redelsperger (2004), The simulation of the diurnal cycle of convective precipitation over land in global model, *Q. J. R. Meteorol. Soc.*, *130*, 3119–3137.

Bony, S., and K. A. Emanuel (2005), On the role of moist processes in tropical intraseasonal variability: Cloud-radiation and moisture-convection feedbacks, *J. Atmos. Sci.*, *62*, 2770–2789.

Carbone, R. E., and J. D. Tuttle (2008), Rainfall occurrence in the U.S. warm season: The diurnal cycle, *J. Clim.*, *21*, 4132–4146.

Chikira, M. (2010), A cumulus parameterization with state-dependent entrainment rate. Part II: Impact on climatology in a general circulation model, *J. Atmos. Sci.*, *67*, 2194–2211.

Collier, J. C., and K. P. Bowman (2004), Diurnal cycle of tropical precipitation in a general circulation model, *J. Geophys. Res.*, *109*, D1705, doi:10.1029/2004JD004818.

Dai, A. G. (2006), Precipitation characteristics in eighteen coupled climate models, *J. Clim.*, *19*, 4605–4630.

Dai, A. G., and K. Trenberth (2004), The diurnal cycle and its depiction in the Community Climate System Model, *J. Clim.*, *17*, 930–951.

Dai, A. G., F. Giorgi, and K. E. Trenberth (1999), Observed an model-simulated diurnal cycles of precipitation over the contiguous United States, *J. Geophys. Res.*, *104*, 6377–6402.

Del Genio, A. D., and J. Wu (2010), The role of entrainment in the diurnal cycle of continental convection, *J. Clim.*, *23*, 2722–2738.

Derbyshire, S. H., I. Beau, P. Bechtold, J. Y. Grandpeix, J. M. Piriou, J. L. Redelsperger, and P. M. M. Soares (2004), Sensitivity of moist convection to environmental humidity, *Q. J. R. Meteorol. Soc.*, *130*, 3055–3079.

de Rooy, W. C., P. Bechtold, K. Fröhlich, C. Hohenegger, H. Jonker, D. Mironov, A. P. Siebesma, J. Teixeira, and J. I. Yano (2013), Entrainment and detrainment in cumulus convection: An overview, *Q. J. R. Meteorol. Soc.*, *139*, 1–19, doi:10.1002/qj.1959.

Hohenegger, C., and C. S. Bretherton (2011), Simulating deep convection with a shallow convection scheme, *Atmos. Chem. Phys.*, *11*, 10,389–10,406, doi:10.5194/acp-11-10389-2011.

Hohenegger, C., P. Brockhaus, C. S. Bretherton, and C. Schär (2009), The soil moisture-precipitation feedback in simulations with explicit and parameterized convection, *J. Clim.*, *22*, 5003–5020.

Hourdin, F., et al. (2013), LMDZ5B: The atmospheric component of the IPSL climate model with revisited parameterizations for clouds and convection, *Clim. Dyn.*, *40*, 2193–2222, doi:10.1007/s00382-012-1343-y.

Huffman, G. J., R. F. Adler, D. T. Bolvin, G. J. Gu, E. J. Nelkin, K. P. Bowman, Y. Hong, E. F. Stocker, and D. B. Wolff (2007), The TRMM multisatellite precipitation analysis (TMPA): Quasi-global, multiyear, combined-sensor precipitation estimates at fine scales, *J. Hydrometeorol.*, *8*, 38–55.

Khairoutdinov, M., and D. Randall (2006), High-resolution simulation of shallow-to-deep convection transition over land, *J. Atmos. Sci.*, *63*, 3421–3436.

Kuang, Z., and C. S. Bretherton (2006), A mass-flux scheme view of a high-resolution simulation of a transition from shallow to deep cumulus convection, *J. Atmos. Sci.*, *63*, 1895–1909.

Lee, M.-I., S. D. Schubert, M. J. Suarez, J.-K. E. Schemm, H.-L. Pan, J. Han, and S.-H. Yoo (2008), Role of convection triggers in the simulation of the diurnal cycle of precipitation over the United States Great Plains in a general circulation model, *J. Geophys. Res.*, *113*, D02111, doi:10.1029/2007JD008984.

Lee, M.-I., S. D. Schubert, M. J. Suarez, T. L. Bell, and K.-M. Kim (2007a), Diurnal cycle of precipitation in the NASA Seasonal to Interannual Prediction Project atmospheric general circulation model, *J. Geophys. Res.*, *112*, D16111, doi:10.1029/2006JD008346.

Lee, M. I., S. D. Schubert, M. J. Suarez, I. M. Held, N. C. Lau, J. J. Ploshay, A. Kumar, H. K. Kim, and J. K. E. Schemm (2007b), An analysis of the warm-season diurnal cycle over the continental United States and northern Mexico in general circulation models, *J. Hydrometeorol.*, *8*, 344–366.

Lynn, B. H., L. Druyan, C. Hogrefe, J. Dudhia, C. Rosenzweig, R. Goldberg, D. Rind, R. Healy, J. Rosenthal, and P. Kinney (2004), Sensitivity of present and future surface temperatures to precipitation characteristics, *Clim. Res.*, *28*, 53–65.

Mauritsen, T., et al. (2012), Tuning the climate of a global model, *J. Adv. Model. Earth Syst.*, *4*, M00A01, doi:10.1029/2012MS000154.

Möbis, B., and B. Stevens (2012), Factors controlling the position of the ITCZ on an aquaplanet, *J. Adv. Model. Earth Syst.*, *4*, M00A04, doi:10.1029/2012MS000199.

Morton, B. R., G. Taylor, and J. S. Turner (1956), Turbulent gravitational convection from maintained and instantaneous sources, *Proc. R. Soc. London, Ser. A*, *234*, 1–23.

Nesbitt, S. W., and E. J. Zipser (2003), The diurnal cycle of rainfall and convective intensity according to three years of TRMM measurements, *J. Clim.*, *16*, 1456–1475.

Nordeng, T. E. (1994), Extended versions of the convective parameterization scheme at ECMWF and their impact on the mean and transient activity of the model in the tropics, Tech. Rep. 206, ECMWF, Reading.

Oueslati, B., and G. Bellon (2013), Convective entrainment and large-scale organization of tropical precipitation: Sensitivity of the CNRM-CM% hierarchy of models, *J. Clim.*, *26*, 2931–2946.

Rio, C., F. Hourdin, J. Y. Grandpeix, and J. P. Lafore (2009), Shifting the diurnal cycle of parameterized deep convection over land, *Geophys. Res. Lett.*, *36*, L07809, doi:10.1029/2008GL036779.

Simpson, J. (1971), On cumulus entrainment and one-dimensional models, *J. Atmos. Sci.*, *28*, 449–455.

Simpson, J., and V. Wiggert (1969), Models of precipitating cumulus towers, *Mon. Weather Rev.*, *97*, 471–489.

Stephens, G. L., M. Wild, P. W. Stackhouse, T. L'Ecuyer, S. Kato, and D. S. Henderson (2012), The global character of the flux of downward longwave radiation, *J. Clim.*, *25*, 2329–2340.

Stevens, B., et al. (2013), Atmospheric Component of the MPI-M Earth System Model: ECHAM6, *J. Adv. Model. Earth Syst.*, *5*, 146–172, doi:10.1002/jame.20015.

Stirling, A. J., and R. A. Stratton (2012), Entrainment processes in the diurnal cycle of deep convection over land, *Q. J. R. Meteorol. Soc.*, *138*, 1135–1149, doi:10.1002/qj1868.

Stratton, R. A., and A. J. Stirling (2012), Improving the diurnal cycle of convection in GCMs, *Q. J. R. Meteorol. Soc.*, *138*, 1121–1134, doi:10.1002/qj.991.

Taylor, K. E. (2001), Summarizing multiple aspects of model performance in single diagram, *J. Geophys. Res.*, *106*, 7183–7192.

Tiedtke, M. (1989), A comprehensive mass flux scheme for cumulus parameterization in large-scale models, *Mon. Weather Rev.*, *117*, 1779–1800.

Wang, Y., L. Zhou, and K. Hamilton (2007), Effect of convective entrainment/detrainment on the simulation of the tropical precipitation diurnal cycle, *Mon. Weather Rev.*, *135*, 567–585.

Wernli, H., M. Paulat, M. Hagen, and C. Frei (2008), SAL-A novel quality measure for the verification of quantitative precipitation forecasts, *Mon. Weather Rev.*, *136*, 4470–4487.

Xie, S., M. Zhang, J. S. Boyle, R. T. Cederwall, G. L. Potter, and W. Lin (2004), Impact of a revised convective triggering mechanism on Community Atmospheric Model Version 2 simulations: Results from short-range weather forecasts, *J. Geophys. Res.*, *109*, D14102, doi:10.1029/2004JD004692.

Yang, Y., and J. Slingo (2001), The diurnal cycle in the tropics, *Mon. Weather Rev.*, *129*, 784–801.

Zhang, G. J. (2003), Roles of tropospheric and boundary layer forcing in the diurnal cycle of convection in the U.S. southern great plains, *Geophys. Res. Lett.*, *30*, 2281, doi:10.1029/2003GL018554.